Electromagnetic simulation and beam-pattern optimization of a C-band Phased Array Feed for the Sardinia Radio Telescope

Alessandro Navarrini
INAF-Cagliari Astronomy Observatory
Selargius, Italy
alessandro.navarrini@inaf.it

Renzo Nesti
INAF-Arcetri Astrophysical Observatory
Florence, Italy
nesti@arcetri.astro.it

Luca Schirru
INAF-Cagliari Astronomy Observatory
Selargius, Italy
luca.schirru@inaf.it

***Abstract*—We report on results of electromagnetic co-simulations and beam-pattern optimization of the C-band PHAROS (PHased Arrays for Reflector Observing Systems) Phased Array Feed (PAF) from the primary focus of the 64-m diameter Sardinia Radio Telescope (SRT). We calculated the radiation patterns of a sub-array of 24 PHAROS Vivaldi array elements and propagated them through the reflector. We present the SRT far-field beam patterns obtained by linearly combining different PAF sub-array configurations with uniform weights. Furthermore, we used the Conjugate Field Matching (CFM) technique to derive optimum beam weights to maximize the SRT on-axis gain. The results show that the PHAROS array could be used at the focus of the SRT to provide high antenna performance, with high-quality illumination and efficiency greater than 60% across 4-8 GHz.**

Keywords—receiver, phased array feed, conjugate field matching, beam-forming, radio astronomy

I. INTRODUCTION

High-sensitivity large-scale surveys are an essential tool for new discoveries in radio astronomy. A PAF placed at the focal plane of an antenna can increase the Field-of-View (FoV) and the mapping efficiency by fully sampling the sky [1]-[2]-[3]. A PAF consists of closely packed antenna elements with about half wavelength element separation that, by spatially sampling the focal plane, can synthesize multiple independent beams and be set to Nyquist-sample the sky. Multiple beams are formed by electronically adding the signals from different groups of radiating elements of the array. An antenna element can contribute to form multiple beams. The properties of the beams can be optimized over a wide range of frequencies by electronically controlling each element phase and amplitude (complex weights) leading to high aperture efficiency and low spillover.

Fig. 1 depicts a Focal Plane Array (FPA) at the primary focus of a telescope and shows that plane waves from different sky directions are focused on different areas of the FPA. The linear size of the electric field distribution on the focal plane is of order $f\lambda/D$, where λ is the wavelength, D the telescope aperture diameter and f its focal length. For a given direction θ, within a relative small region (FoV) close to the boresight direction, it is possible to maximize the coupling to a plane wave without a significant efficiency loss using a suitable illumination of the telescope aperture that provides a wavelength-dependent telescope resolution, in terms of Half Power Beam Width (HPBW) given by $\theta_{3dB} \approx \lambda/D$. Instead, in first approximation, the angle of the off-axis far-field direction θ with respect to the boresight is wavelength-independent and scales as the ratio $\theta \approx d/f$, where d is the distance from the on-axis geometrical focus and the area of the focal plane excited by the off-axis source (location of the focal field distribution due to the incoming off-axis wave). Therefore, multiple beams can be pointed to different directions on the sky by suitably exciting different focal plane areas (different sub-arrays of the FPA). The antennas on the focal plane array have to be designed to efficiently sample the focal plane fields and to avoid generation of grating lobe responses, while minimizing the noise performance of the receiver chains (by accounting of mutual coupling effects).

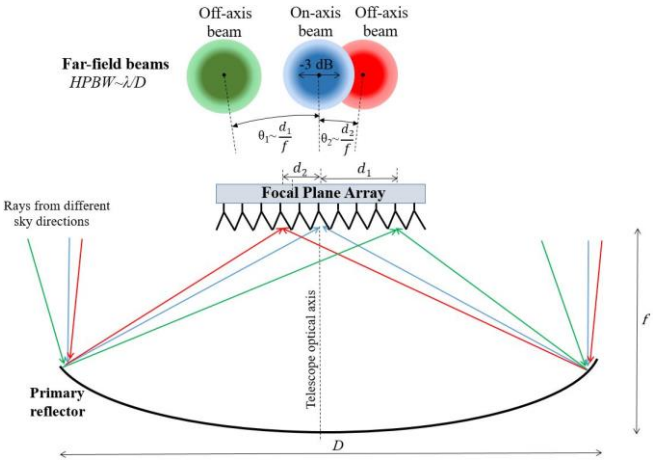

Fig. 1. Bottom: Schematic of a FPA at the primary focus of an axially symmetric single dish parabolic reflector with diameter D and focal length f. Plane waves from three different sky directions (on-axis in blue, off-axis in green and red) excite different areas of the FPA. Top: Far field patterns (angular size ≈λ/D) and angular displacements from boresight (≈d/f) resulting from the excitation of the different areas of the FPA at distance d from the axis.

In this paper, we present the results of the electromagnetic simulations aimed at optimizing the weights of sub-array elements of the PHAROS phased array feed illuminating the SRT from primary focus. An introduction to PHAROS and SRT is given below.

A. PHAROS Focal Plane Array

PHAROS [4]-[5] is a cryogenically cooled 4-8 GHz PAF technology demonstrator with four analogue beamformers designed for radio astronomy application. The PHAROS system architecture is shown in Fig. 2. The instrument consists of a focal plane array of 10×11 dual polarization Vivaldi antennas (total of 220 radiating elements, Fig. 3) cooled to 20 K along with 24 low noise amplifiers (LNAs) mounted directly behind the array elements. The LNAs are

cascaded with four analogue beam formers [6], based on MMIC [7], designed to operate at 77 K. The RF signals of the 24 active elements are distributed to four beam formers by passive splitters, while the non-active elements are terminated into 50 Ω loads. The non-active elements add negligible noise contribution due to their low operating

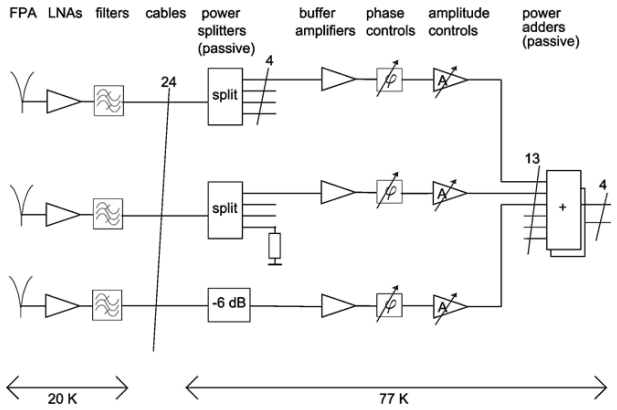

Fig. 2. Schematic diagram of PHAROS: 24 active elements of the cryogenic focal plane array are distributed to four analogue beamformers.

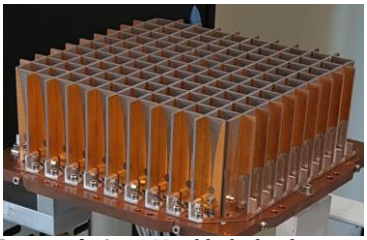

Fig. 3. PHAROS array of 10×11 Vivaldi dual polarization antennas. Only the 24 central elements of the array are used to beamforming, the rest are matched terminated.

temperature of 20 K. Each beam former has 13 RF inputs and consists of 13 individually controllable phase and amplitude control units and of 13 amplifiers to compensate for system losses. The last stage of beam forming is a 13-way combiner (16-way Wilkinson combiner with three terminated inputs). Each analogue beam former applies amplitude and phase weights to each of the 13 elements in order to produce a single (compound) one-polarization beam.

PHAROS is being upgraded to PHAROS2 [8], a new PAF with *digital* beamformer that re-uses parts of the existing hardware, including the array of Vivaldi antennas. PHAROS2 is under development by an international collaboration in the framework of the SKA (Square Kilometer Array) PAF Advanced Instrumentation Program. The goal of the upgrade is to reduce the system noise and to digitize the signals from the sub-array of 24 Vivaldi antenna elements, following downconversion and bandpass filtering by a "warm section" receiver. The PHAROS2 digital backend synthesizes four independent single-polarization beams across a 275 MHz instantaneous bandwidth. Unlike PHAROS, PHAROS2 employs all of the 24 sub-array elements to synthesize the beams (not only 13 elements per beam).

B. *The Sardinia Radio Telescope*

The SRT (www.srt.inaf.it), a challenging scientific project of the Italian National Institute for Astrophysics (INAF), is a new general purpose fully steerable 64-m diameter radio telescope designed to operate with high efficiency across the 0.3-116 GHz frequency range [9]. Since Dec. 2018 the telescope (Fig. 4) has been opened to the international community to carry out radio astronomy observing programs [10]. The SRT optical design is based on a quasi-Gregorian configuration (Fig. 5) with shaped 64 m diameter primary (M1) and 7.9 m diameter secondary (M2) reflectors to minimize spillover and standing waves. The primary mirror utilizes an active surface with electromechanical actuators to compensate the gravitational deformation and convert the shaped surface to parabolic during primary focus observation. The telescope has been designed to host receivers at six focal positions: Primary focus (F1), Gregorian focus (F2) and Beam-Wave Guide foci (F3&F4 and F5&F6). The focal length to diameter ratio at the primary is *f/D*=0.33. The Front-Ends currently installed on SRT and the future perspectives for developing and installing a PAF at the SRT primary focus are described in [11].

Fig. 4. Sardinia Radio Telescope at the opening ceremony in Sep. 2013.

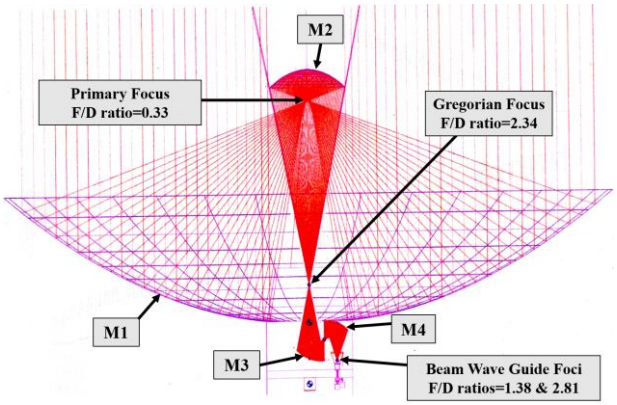

Fig. 5. Optical configuration and ray tracing of the SRT showing the 64-m diameter primary (M1), the 7.9-m secondary (M2), and two additional Beam Waveguide (BWG) mirrors (M3 and M4). Three out of six possible focal positions (primary, Gregorian and BWG) are shown together with corresponding focal ratios.

II. PHAROS Electromagnetic Simulations

A. *3D simulation of PHAROS Vivaldi array and beam pattern (without coupling to the SRT optics)*

The PHAROS Vivaldi array shown in Fig. 3 utilizes high-performance Taconic PCBs (TLY-5 substrate, with ε_r=2.20, tanδ=0.0008). A three layer laminated board structure, based on two 1.14 mm thick substrates was employed [4]. The antenna feed element is a stripline on the center conductor layer, sandwiched between the two board

laminates. Fig. 6 shows the 3D structure of the array that we simulated with the commercial electromagnetic software CST Microwave Studio (https://www.cst.com). The complete PHAROS FPA antenna was built with 11 boards in both the *x* and the *y* directions, each integrating 10 Vivaldi elements with 21 mm spacing. The spacing-to-wavelength ratio is 0.56 at the PHAROS maximum operating frequency of 8 GHz (λ_{min}≈37.5 mm). The overall size of the array on the *x*-*y* plane is ≈230×230 mm^2, i.e. ≈6λ_{min}×6λ_{min} (and equivalently ≈3λ_{max}×3λ_{max} for λ_{max}≈75 mm, relative to the 4 GHz minimum frequency).

The CST model of the array employs 220 ports, 110 per polarization channel (Fig. 7). We excited the 24 active stripline ports of the *y*-polarization antennas of the array. These are the ports selected to be cascaded with LNAs and used for synthesizing the four beams. We calculated the S-parameters and far-field patterns generated by each Vivaldi element using the time domain solver. The model used ≈6 million meshcells. We made sure that all the stripline ports and the most critical parts of the antennas, where the highest electric field energy density is expected, were sufficiently well meshed. The computation time for the 24 ports was of order one week on a fast PC equipped with 64 GB RAM memory. The impedance of the ports is ≈33 Ω.

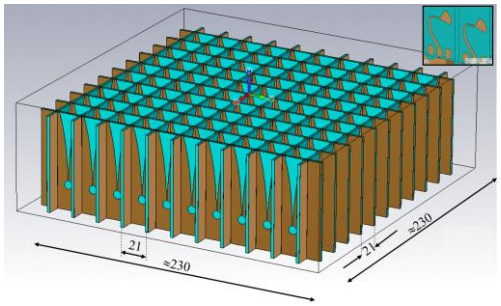

Fig. 6. CST model of the PHAROS array of 10×11 dual-polarization Vivaldi antenna elements with Taconic board substrates. Dimensions are in mm. The inset on the top right shows the detail of two of the antenna stripline feed elements.

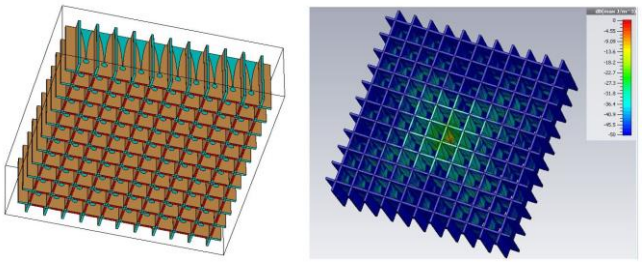

Fig. 7. Left: 3D model of the PHAROS array showing the 220 stripline ports. Right: Simulated electric energy distribution of PHAROS when exciting one of the central antenna elements (Ant. #175) aligned along the y direction at 6 GHz. The intensity of the energy distribution is color-coded through the scale given on the top right.

1) Far-field of a single Vivaldi element of the array

The right panel of Fig. 7 shows the simulation results of the electric energy distribution at 6 GHz obtained by the excitation of one of the central elements of the array (Ant. #175). A relatively strong mutual coupling with the nearby elements is visible from the colour-scale image. The simulated far-field patterns of that array element at 4, 6 and 8 GHz are shown in Fig. 8. The copolar (CP) patterns are symmetric with respect to the boresight angle on the different cuts. The left side of Fig. 9 plots the associated copolar and cross polar (CX) antenna gains versus boresight angle (for the *y* polarization). The boresight gains are around 6 dBi at the three frequencies, while the HPWB are weakly frequency-dependent and have a value of ≈50 deg at the three simulated frequencies.

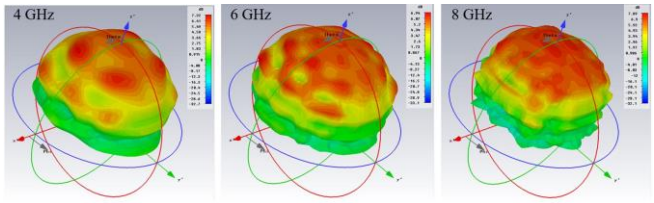

Fig. 8. 3D far-field beam pattern from Vivaldi element #175 at 4, 6 and 8 GHz simulated with CST.

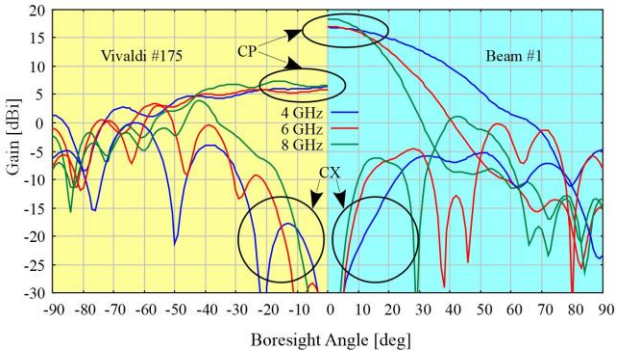

Fig. 9. Simulated antenna gains from Vivaldi element #175 (left side plots) versus Beam #1 (right side plots) formed by a linear combination of 13 elements equally fed. The plots refer to three following frequencies: 4 GHz (blue curve), 6 GHz (red curve) and 8 GHz (green curve).

2) Far-field of 13 Vivaldi elements combined

We simulated, using CST, the far-field patterns of the 24 active Vivaldi antenna elements. The PHAROS 24-element subarray was designed to form four independent beams, each utilizing a subset of 13 elements, as illustrated in Fig. 10. We uniformly excited the elements of the 13-element subarrays using unitary-power normalized-weights, i.e. all equally fed in amplitude and phase. Fig. 11 shows the resulting far-field beam patterns of one of the formed beams (Beam #1). The right side of Fig. 9 plots the associated copolar and cross-polar antenna gains versus boresight angle. The boresight gains are around 17 dBi at the three frequencies, and the HPBW are frequency dependent and of order 18 deg at 6 GHz. We note that the antenna gain difference between the single element (≈6 dBi) and the 13-element sub-array (≈17 dBi) is as expected from array theory (-11.139 dB, or 1/13 in linear power scale).

III. Co-Simulation of the PHAROS Array at the SRT Primary Focus and Coupling with the Reflector

We performed electromagnetic co-simulations of the PHAROS FPA at the primary focus of the 64-m SRT dish (*f*/*D* =0.33), as depicted in Fig. 12. We modelled the SRT primary reflector M1 with the commercial software GRASP (https://www.ticra.com). In particular, we coupled the CST simulated far-fields generated by the 24 active Vivaldi antenna elements (at 4, 6 and 8 GHz) to the SRT optics using the GRASP PO/PTD solvers (the output far-field files from CST were imported into GRASP). We used a simplified GRASP model for SRT: we assumed an ideal primary reflector with parabolic profile that has no quadrupod and includes no blockage due to the secondary mirror M2. The GRASP simulation for the three frequencies runs in approximately 12 hours. Then, the GRASP output files were

imported into a Matlab (http://www.mathworks.com) script, developed to generate the final *uv* far-field plots of all the following figures.

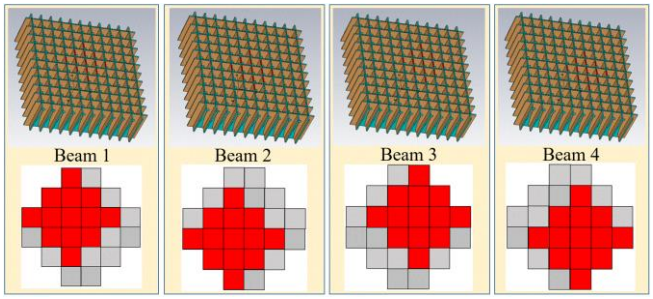

Fig. 10. Subsets of 13 Vivaldi elements of the 24 active antennas used to synthesize the four beams (Beam #1 to Beam #4).

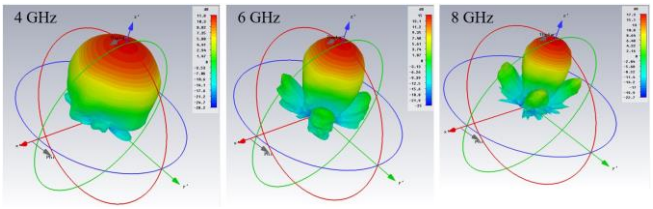

Fig. 11. 3D far-field beam patterns of Beam #1 obtained from 13 Vivaldi antenna elements equally fed both in amplitude and in phase at 4, 6, 8 GHz.

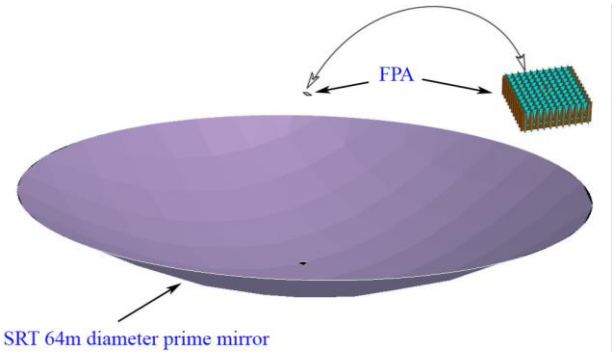

Fig. 12. Illustration of the CST-GRASP co-simulation adopted for modelling the PHAROS Focal Plane Array at the primary focus of SRT.

We note that the M1 edge is seen from the primary focus under a 74 deg half-angle. Thus, a suitable illumination pattern of M1 from primary is required to cover an angle of order 150 deg. For example, a typically used dish illumination is a Gaussian taper, which maximizes the aperture efficiency at $A_{eff}\approx0.8$ with about 11 dB level edge taper [12]. The maximum is obtained as a trade-off between the illumination efficiency and the spillover efficiency.

1) Far-field of a single Vivaldi element of the array coupled to SRT

Each FPA Vivaldi element generates a specific far-field beam pattern on the sky when coupled to the SRT reflector. Fig. 13 shows the *uv* plots of the copolar and cross-polar far-field patterns obtained by illuminating the SRT with a single Vivaldi element of the array (Ant. #175) at 4, 6 and 8 GHz. Related performance parameters of this CST-GRASP co-simulation are listed in Table I, third column. The antenna gain is in the range 66.9-71.34 dBi, while the antenna efficiency varies from 47% (at 8 GHz) to 65% (at 4 GHz). We note that the simulated HPBW match well with the values we estimate with the simplified formula $HPBW\approx1.22\,\lambda/D$ (4.91 arcmin at 4 GHz, 3.27 arcmin at 6 GHz, and 2.45 arcmin at 8 GHz). The cross-polarization plots, shown on the right panel of Fig. 13, have maxima at 45-degree azimuthal angle. The cross-pol values are in the range -11.59 dB to -17.59 dB below the maximum of the copolar gain.

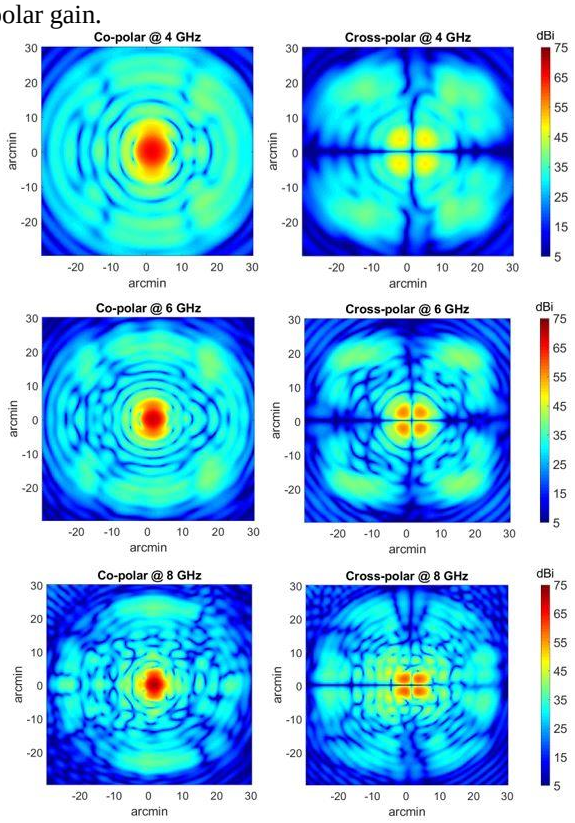

Fig. 13. Vivaldi element # 175 at SRT primary focus: co-polar (left) and cross-polar (right) beams on the sky at 4 GHz (top), 6 GHz (center) and 8 GHz (bottom).

TABLE I. SIMULATED PARAMETERS OF THE SRT ANTENNA ILLUMINATED BY: A SINGLE VIVALDI ELEMENT (ANT. #175); 13 EQUALLY FED ELEMENTS; 24 EQUALLY FED ELEMENTS; 24 ELEMENTS WITH CFM-DERIVED WEIGHTS.

	Freq. [GHz]	Ant. #175	13 ants. equally fed	24 ants. equally fed	CFM weights
SRT gain [dBi]	4	66.69	70.12	65.89	72.31
	6	69.78	64.77	63.07	72.62
	8	71.34	64.02	61.77	72.36
SRT efficiency A_{eff} [%]	4	65	143	54	237
	6	57	19	12	113
	8	47	9	5	60
HPBW [arcmin]	4	4.82	6.23	13.5	5.0
	6	3.27	N.A.*	N.A.*	3.2
	8	2.66	N.A.*	N.A.*	3.1
Cross-pol [dB]	4	-17.59	-24.04	-23.97	-19.32
	6	-12.94	-15.06	-12.95	-14.81
	8	-11.59	-11.53	-12.88	-14.18

*Not Applicable because the beam has multiple maxima.

2) Far-field of 13 Vivaldi elements coupled to SRT

The far-fields of each of the 24 active Vivaldi antenna elements were propagated through the reflector. We formed four SRT far-field beams, each resulting from a linear combination of the antenna patterns generated by the sub-set of 13 Vivaldi elements illustrated in Fig 10. The 2D plots of the co-polar and cross-polar far-field patterns of Beam #1, obtained by a power-normalized equal-weight combination of the responses from the 13 Vivaldi antennas, are shown in Fig. 14. The derived antenna parameters are summarized in

Table I, fourth column. At 4 GHz the reflector is under-illuminated, but the overall pattern and efficiency are sufficiently good. Instead, at 6 GHz and 8 GHz the antenna efficiencies drop to very low level as a result of a strong under illumination of the reflector, due to the narrow beams produced by the combination of 13 equally-weighted antennas. This behaviour had to be expected by the results of Fig. 9, showing field levels at 74 deg (edge taper), respectively ≈20 dB, ≈32 dB and ≈38 dB below on-axis values. While at 4 GHz the HPBW=6.23 arcmin is larger than expected from optimum aperture illumination and can be sufficiently well defined, it was not possible to estimate such antenna parameter at 6 GHz and 8 GHz because the beams have multiple maxima.

We note that the antenna efficiency at 4 GHz, calculated with GRASP, is greater than 1 (143%). This apparent element-gain paradox of phased array antennas was discussed in [13]. We can explain this result by considering the transmission mode and assuming that, when computing efficiency comparison for a PAF and a single feed, the same unitary power should be provided at their inputs. We can realize that the value of the array efficiency is normalized to the power that would be given to a single antenna element: as we employ 13 antennas, with the same power fed to a single element divided by 13, it is possible to achieve efficiencies greater than 100%. If we renormalize the array pattern we would obtain antenna efficiencies less than 100%, but we would also have less power compared to the one fed into a single antenna element. Therefore, the comparison is made assuming that equal power is provided to the array and to the single Vivaldi element and that the reference isotropic power is 4π W.

The simulated far field patterns of Beam #2, #3 and #4, are very similar to those of Beam #1 shown in Fig. 14. The difference is in the beam-spot directions. The GRASP simulated result for the angular separation between the maxima of two equal-weight beams (for example Beam #1 and Beam #2) is ≈2.7 arcmin (frequency independent). This is close to the expected value of $\theta \approx d_{el}/f$=3.4 arcmin, with f=21 m (the SRT primary focal length), due to the separation between the two associated sub-arrays on the focal plane, equal to the Vivaldi element size (d_{el}=21 mm).

IV. Conjugate Field Matching applied to PHAROS-SRT

The conjugate field matching method (CFM) is a technique to derive the optimum PAF element weights and maximize the coupling between a plane wave from a given direction and the receiver signal [14]. Since the prime mirror capturing the incident plane wave has a circular aperture, the on-axis beam has, on the focal plane, the typical diffraction figure of a circular aperture known as Airy pattern [15]. Off-axis beams or aberrated (distorted) mirrors would result in focal plane field distributions different from the Airy pattern. The basis for the CFM method is the fact that the product of a phase-distorted field and its complex conjugate is a plane wave. This opens the possibility to use PAFs for dish distortion compensation and for correction of off-axis aberrations. Once a focal plane field distribution E_i produced by a plane wave illuminating the reflector is known, the weighting field distribution E_w producing maximum flux of energy $E_w \cdot E_i$ on the focal plane is its complex conjugate $E_w=E_i^*$. Since an array can be thought as a discrete sampler of a focal plane field, the optimum coupling excitation coefficients for delivering maximum power are the complex

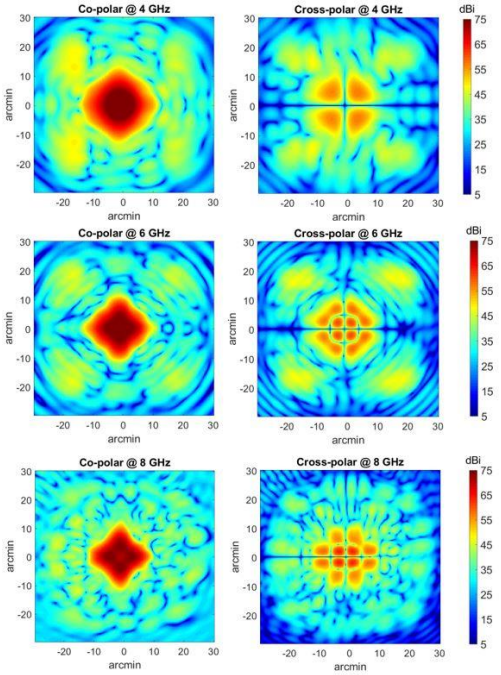

Fig. 14. Beam #1 patterns on the sky obtained by adding the far-field responses of 13 Vivaldi antenna elements feeding the SRT reflector from primary focus. Equal-weight was used to add the 13 far-fields. Co-polar (left) and cross-polar (right) beams on the sky at 4 GHz (top), 6 GHz (center) and 8 GHz (bottom).

conjugate of the field samples at each element position. Due to the reciprocity theorem the focal plane field in receiving mode can be estimated from the far-field in transmitting mode: the samples of the Airy pattern (or focal plane phase distorted field samples) can be obtained by considering each array element in transmission, illuminating the reflector system, and calculating the field at a given far-field distance in the same direction as the incoming plane wave under consideration. The samples obtained in this way are complex numbers for which it is important to preserve their relative distribution.

We derived the CFM optimum beam weights of the 24 PHAROS active antenna elements for SRT boresight illumination using Matlab. The conjugate of the simulated boresight far-field values gave the CFM complex weights, which we evaluated at 4, 6 and 8 GHz. The moduli of the derived weights are plotted in Fig. 15. We used the 24 derived CFM weights to generate the *uv* SRT co-polar (Fig. 16, right panels) and cross-polar (Fig. 17, right panel) beam patterns. For comparison, the left panels of Figs. 16 and 17, show the co-polar and cross-polar beam patterns that would be obtained by equal-weight illumination of the 24 Vivaldi antenna elements. The summary of the results, provided in Table I, shows how the CFM weights achieve high antenna performance with gain greater than 72 dBi and efficiency as high as 60% at 8 GHz. Efficiencies of 237% and 113% are obtained at 4 GHz and 6 GHz, respectively.

V. Conclusion

We reported on electromagnetic co-simulations and beam-pattern efficiency optimization of PHAROS from the primary focus of the SRT. No attempts was made to control

the antenna sidelobe level, but we focused on maximizing the coupling to a plane wave from boresight using the CFM method. By comparing the far-field differences obtained by feeding SRT with: *a)* 24 equal-weight Vivaldi elements; *b)* an optimized weight procedure based on CFM, it appears that the SRT efficiency increases from 54% to 237% at 4 GHz, from 12% to 113% at 6 GHz and from 5% to 60% at 8 GHz. This aspect demonstrates that the CFM method might be used to achieve a performances boost of the SRT when equipped with a Phased Array Feed like PHAROS.

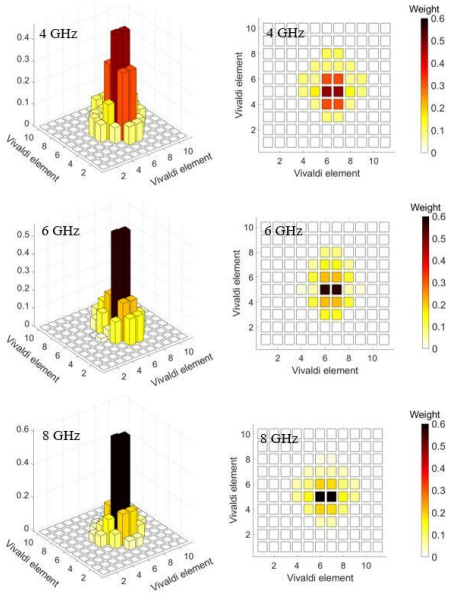

Fig. 15. Weights of the 24 antennas calculated by CFM at 4 GHz (top), 6 GHz (center) and 8 GHz (bottom).

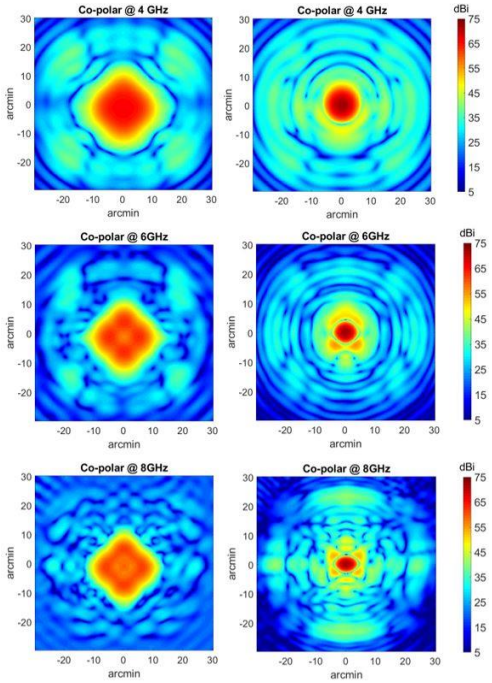

Fig. 16. Co-polar beam patterns of SRT by feeding 24 Vivaldi antennas with equal-weight (left panels) and with CFM weigths (right panels) at 4 GHz (top), 6 GHz (center) and 8 GHz (top).

REFERENCES

[1] J.R. Fisher, R.F. Bradely, "Full-sampling array feeds for radio telescopes," Proceedings of SPIE Astronomical Telescopes and Instrumentation, Vol 4015, 2000.

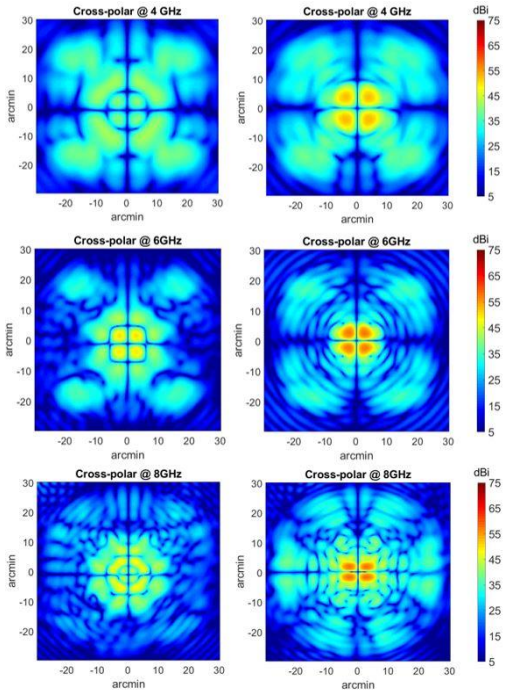

Fig. 17. Cross-polar beam patterns of SRT by feeding 24 Vivaldi antennas with equal-weight (left panels) and with CFM weights (right panels) at 4 GHz (top), 6 GHz (center) and 8 GHz (top).

[2] K. Warnick, R. Maaskant, M.V. Ivashina, D.B. Davidson, B.D. Jeffs, "High-Sensitivity Phased Array Receivers for Radio Astronomy, Proceedings of the IEEE, Vol. 104, Issue 3, pp. 607-622, March 2016.

[3] D. Anish Roshi et al., "Performance of a highly sensitive, 19-element, dual-polarization, cryogenic L-band phased array feed on the Green Bank Telescope," The Astronomical Journal, 155:202, May 2018.

[4] J. Simons et al. "Design of a focal plane array system at cryogenic temperatures," Proc. 'EuCAP 2006', Nice, France, 6–10 Nov. 2006.

[5] L. Liu, K. Grainge, and A. Navarrini, "Analysis of Vivaldi array antenna for phased array feeds application," presented at the IEEE MTT-S Int. Conf. on Num. Electr. and Multiphysics Modeling and Opt. for RF, Microwave, and Terahertz Applications (NEMO), 2017.

[6] J. Simons, M. Ivashina, J. G. b. d. Vaate, and N. Roddis, "Beamformer system model of focal plane arrays in deep dish radio telescopes," in 2005 European Microwave Conf., 2005, vol. 3, p. 4.

[7] W. Ciccognani, F. Di Paolo, F. Giannini, E. Limiti, P.E. Longhi, A. Serino, "A GaAs Front-end Receiver for Radio Astronomy Applications," 13th IEEE Melecon 2006, May 16-19, Spain.

[8] A. Navarrini et al. "Design of PHAROS2 Phased Array Feed," Proceedings of 2nd URSI Atlantic Radio Science Meeting (AT-RASC), 28 May –1 June 2018.

[9] G. Grueff et al., *Sardinia Radio Telescope: The new Italian project*, Proc. SPIE Ground Based Telescopes, Vol. 5489, p. 773, 2004.

[10] I. Prandoni et al. "The Sardinia Radio Telescope: From a Technological Project to a Radio Observatory," Astronomy & Astrophysics, 2017, A&A, 608, A40.

[11] A. Navarrini et al. "Front-Ends and Phased Array Feeds for the Sardinia Radio Telescope," Proceedings of 32nd URSI GASS, Montreal, 19-26 August 2017.

[12] P. Goldsmith, "Quasioptical Systems: Gaussian Beam Quasioptical Propogation and Application," Wiley IEEE press, 1998. ISBN-13: 978-0780334397.

[13] P. Hannan, "The Element-Gain Paradox for a Phased-Array Antenna," IEEE Transactions on Antennas and Propagation, Vol. 12, Issue 4, July 1964, p. 423-433.

[14] Y. Rahmat-Samii, "Array feeds for reflector surface distortion compensation: Concepts and implementation," IEEE Antennas Propag. Mag., pp. 20–26, Aug. 1990.

[15] Airy, G. B. (1835). "On the Diffraction of an Object-glass with Circular Aperture". *Transactions of the Cambridge Philosophical Society* p. 283-91.